


Polarization-dependent reflection of I-WP minimal-surface-based photonic crystalRyosuke Ohnuki ,* Yuka Kobayashi, and Shinya Yoshioka*Graduate School of Science and Technology, Tokyo University of Science, Yamazaki, Noda 278-8510, Japan*

(Received 26 May 2022; accepted 22 June 2022; published 19 July 2022)

Brilliantly colored butterflies and weevils are known to utilize photonic crystals for their coloration. Interestingly, the morphology of such crystals made of cuticle is based on triply periodic minimal surfaces such as gyroid and diamond surfaces. Recently, a different minimal-surface-based photonic crystal, the I-WP surface, was discovered inside the scale of a longhorn beetle. The letter I is derived from expressing the body center symmetry and WP is derived from a wrapped package. It was reported that the brilliant green color is produced by the photonic band gap existing along the [110] direction of this crystal. In this study, the polarization dependence of the reflection from this photonic crystal was investigated. A peculiar reflectance spectrum with two peaks was observed under the crossed polarizers. This characteristic is theoretically reproduced by calculating the reflectance from a finite-sized photonic crystal, and the spectral shape is explained based on the symmetry of the electromagnetic modes. In addition, inspired by this longhorn beetle, a photonic crystal structure consisting of colloidal particles is proposed, which has a similar polarization effect.

DOI: [10.1103/PhysRevE.106.014123](https://doi.org/10.1103/PhysRevE.106.014123)**I. INTRODUCTION**

In nature, many insects and animals such as birds, fish, butterflies, and beetles have bright structural colors. Their colors mainly originate from optical interference from nanostructures with various morphologies [1–4]. The typical examples of a color-causing structure are single thin-layered and multilayered structures in jewel beetles [5–7], butterflies [8–10], and bird feathers [11,12]. In addition to these layered structures, photonic-crystal-like structures have been found, which are periodic in two or three directions with periodicity of several hundred nanometers.

Some insects possess complicated cuticle networks such as a three-dimensional photonic crystal structure. Interestingly, these cuticle networks are based on several types of triply periodic minimal surfaces [13,14]. Many weevil species are reported to have photonic crystals based on a diamond-type minimal surface [15–19], whereas the gyroid minimal-surface-based crystal was found in the scales on butterfly wings [20–24]. These surfaces separate the three-dimensional space into two interconnected channels—one is filled with cuticles whereas the other contains air. These photonic crystals have attracted the attention of many scientists; the diamond-type structure is known to possess the widest full photonic band gap [25], where light with a frequency within the band gap cannot propagate along any direction inside the crystal. In contrast, the gyroid-type photonic crystal has helical axes, as the name implies, and it selectively reflects circularly polarized light with a specific helicity within a certain wavelength range [26,27]. This feature has been already applied to produce an optical component with circular polarization dichroism [28–32].

The existence of these photonic crystals in insects directly indicates that the crystals can be produced in a self-organizing manner [21,33]. Thus, many researchers have attempted to understand the optical effects of these photonic structures found in nature and explore their application to new optical materials.

Several interesting optical properties related to polarization have been discovered in natural structural colors. In some butterfly and moth species, a tilted or curved multilayer structure causes polarization rotation and results in the color-mixing effect [34–36]. Polarization conversion was reported in the diamond-type photonic crystal of a weevil when light was incident along a certain crystal direction [37,38]. In the butterfly wing scale, a beautiful tessellated pattern was observed under the crossed polarizers, which is attributed to many small gyroid crystal domains [39,40]. Recently, we discovered the I-WP minimal-surface-based photonic crystal inside the scales of a longhorn beetle (*Sternotomis callais*) [41]. The name I-WP is derived from the two different networks of I and WP; the letter I is derived from expressing the body center symmetry and WP is derived from a wrapped package [42]. The green color of this longhorn beetle is caused by the orientation preference of the multidomain photonic crystals; the [110] direction is preferably along the surface normal in the basal part of the scale. Considering the above examples, we were naturally interested in the polarization-dependent reflection of this photonic crystal, and performed detailed experimental and theoretical investigations. It was found that the width of the reflection band depends on the direction of polarization under the parallel polarizers. Further, the reflectance spectrum under the crossed polarizers has a peculiar shape with two peaks. These optical properties could be reproduced through theoretical calculations, and a simple physical interpretation about the origin of the polarization properties was provided. Finally, inspired by the longhorn beetle, a photonic crystal

*6220701@ed.tus.ac.jp

consisting of colloidal particles and having similar optical properties is proposed.

II. METHOD

A. Sample and cross-sectional processing

The scale of the longhorn beetle (*Sternotomis callais*) was used to experimentally investigate the I-WP photonic crystal. To avoid complexities due to the surface curvature of the elongated scale, we sectioned the scale to expose the photonic structure and optically examined it. An apparatus called a cross-section polisher (IB-19530CP, JEOL, Tokyo, Japan) was used for the sectioning process, which utilized a broad ion beam, resulting in a very smooth cross section [41].

B. Structural observation

To investigate the internal photonic crystal structure, the exposed surface was observed using a scanning electron microscope (SEM) (JCM-6000, JEOL, Tokyo, Japan). The observation was conducted in the secondary electron mode under the acceleration voltage of 5 keV. To enhance the conductivity of the sample, it was coated with a 7.5-nm-thick layer of osmium using an osmium coater (Neoc-Pro, Mei-wafosis, Tokyo, Japan) before the observation.

C. Polarization-dependent optical observation

A polarizing-filter-equipped optical microscope (BX51, Olympus, Tokyo, Japan) was used for the optical observation. A Xe lamp was used as the light source for the epi-illumination and a charge-coupled device camera (DP25, Olympus, Tokyo, Japan) was used to capture the images. An objective lens with numerical aperture of 0.60 (SLMPlan N, Olympus, Tokyo, Japan) was used for the observation. To examine the polarization-dependent optical properties, a polarizer was inserted to linearly polarize the incident light and an analyzer was inserted to select the polarization for the observation. The observation was performed under parallel or crossed polarizers. By rotating the sample in the plane perpendicular to the optical axis, the direction of the incident polarization was changed with respect to the photonic crystal orientation.

D. Microspectrophotometry

To determine the reflectance spectra of a small region, one edge of an optical fiber was placed on the image plane of the above microscope, and the light reflected from a small region was guided into a fiber optic spectrometer (USB2000, Ocean Optics, Tokyo, Japan). The reflectance spectrum was determined as the ratio of the spectrum of the sample to the spectrum of the dielectric multilayer mirror (Sigma Koki, Tokyo, Japan), which has nearly 100% reflectance over the wavelength range of 320 to 850 nm. A pinhole with a diameter of 200 μm was placed on the aperture stop of the microscope so that the illumination was approximately collimated at the sample position. The maximum incidence angle with respect to the optical axis was approximately 5.7°. A 50 \times objective lens and 200- μm -diameter optical fiber were used

for the measurement; consequently, a measurement spot was a circular region of 4 μm diameter.

E. Photonic band calculation

The photonic band diagram of the I-WP-type photonic crystal was calculated using the plane-wave expansion method [43]. The EM modes were expanded with the plane waves corresponding to the 1055 reciprocal lattice points around the origin in the reciprocal space. This number was confirmed to be sufficient to obtain the converged results of the calculations. The refractive index of the cuticle was set to 1.555 [44], which was experimentally estimated by the Becke line test of the sample. The I-WP photonic crystal structure was modeled as in our previous study [41] by using the formula

$$F(X, Y, Z) \geq t, \quad (1)$$

where $X = \frac{2\pi}{a}x'$, $Y = \frac{2\pi}{a}y'$, and $Z = \frac{2\pi}{a}z'$; x' , y' , and z' are Cartesian coordinates, and a is the lattice constant of the cubic lattice. The spatial region that satisfies the above formula is filled with cuticle. A level-set parameter t on the right-hand side relates to the cuticle fraction and is set to 0.218 [41]. The function $F(X, Y, Z)$ on the right-hand side consists of several terms of sinusoidal functions; in the interest of conciseness, the exact formula is provided in the Supplemental Material [45].

F. Rigorous coupled wave analysis

The reflectance from a finite-sized photonic crystal was calculated by using the rigorous coupled wave analysis (RCWA) method [48,49]. A commercial software (RSoft, DiffractMod) was used for the calculation; the I-WP structure was modeled according to Eq. (1) with a lattice constant of $a = 315$ nm, refractive index of cuticle of 1.555, and parameter $t = 0.218$, which were determined for the longhorn beetle scale in our previous study [41]. The light was assumed to be incident normal to the photonic crystal surface of the (110) plane. The plane-wave expansion in the RCWA method was of the order of ± 5 for the two directions ([001] and $[-110]$ directions) orthogonal to the [110] direction. Along the [110] direction, the structure was modeled as the stack of several thin layers with thickness of 5 nm in the calculation. The crystal thickness was assumed to be 20 or 6 periods.

III. RESULTS

The scales of the longhorn beetle (*Sternotomis callais*) appear brilliantly green, as shown in Fig. 1(a). The basal part of the elongated scale is particularly reflective. Our previous study found that the (110) plane of the I-WP photonic crystal is preferably oriented toward the outside. Sectioning was performed nearly parallel to the surface of the elytrum, and one of the sectioned scales was observed using an optical microscope and SEM; the results are shown in Figs. 1(b) and 1(c), respectively. The optical micrograph appears in various colors, but the basal part of the scale (the right side of the image) is brightly reflective in green. When the exposed surface was observed with SEM under higher magnification, a periodic pattern of oval holes could be observed [Fig. 1(d)],

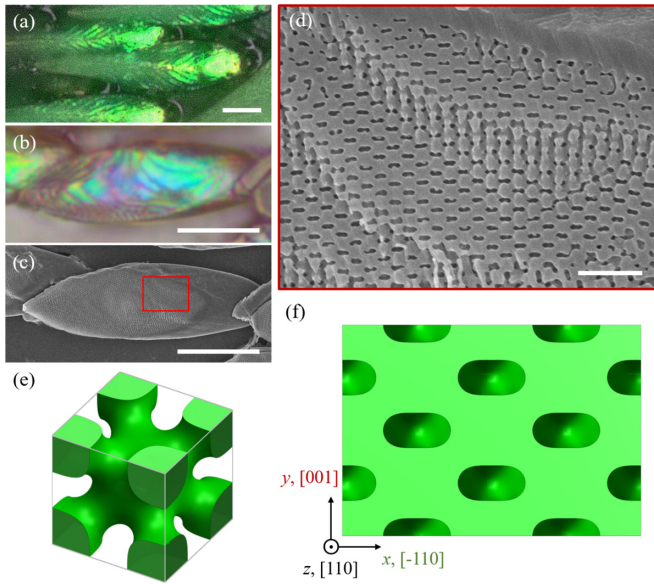


FIG. 1. (a) Optical micrograph of elongated scales of a longhorn beetle (*Sternotomis callais*) before sectioning. (b) Optical micrograph and (c) electron micrograph of a sectioned scale. The scales were sectioned with a broad ion beam. (d) Magnified image of the basal region indicated by the red frame in panel (c). The surface exhibits an arrangement of oval holes corresponding to the (110) plane of the I-WP-type photonic crystal. Scale bars are [(a)–(c)] $10\ \mu\text{m}$ and (d) $1\ \mu\text{m}$. (e) Cubic unit cell of the I-WP-type photonic crystal. (f) (110) plane of I-WP-type photonic crystal. Oval holes are periodically arranged. For the detailed analysis of the polarization dependent properties, we defined the x , y , and z axes along the $[-110]$, $[001]$, and $[110]$ directions, respectively. In these coordinates, the major axis of the oval hole is along the x axis and minor axis is along the y axis.

which corresponded to the (110) plane of the I-WP photonic crystal [Figs. 1(e) and 1(f)] [41]. As the sectioning plane was slightly tilted from the (110) plane, the pattern of the arranged oval holes gradually changed depending on the position. The model calculation that considers the tilt can reproduce this change in the surface texture, as shown in Fig. S1 (see Supplemental Material) [45].

We investigated the polarization-dependent reflective properties of the scale in detail when the light was incident along the $[110]$ direction of the I-WP structure. The incident light was linearly polarized by using a polarizer, and an analyzer was used to select the reflected light with polarization parallel or perpendicular to the incident polarization; this configuration is called the parallel or crossed polarizers, respectively. By rotating the sample in the plane perpendicular to the optical axis, we examined the polarization dependence with respect to the crystal structure. The model calculation using Eq. (1) (see the Method section) reveals that the major and minor axes of the oval holes in the (110) plane are along the $[-110]$ and $[001]$ directions of the I-WP photonic crystal, respectively, as shown in Fig. 1(f). For the detailed analyses, we defined the x , y , and z axes along the $[-110]$, $[001]$, and $[110]$ directions, respectively. To express the direction of incident polarization, we used the polarization angle defined

as the angle between the x axis and the polarization direction of the incident light.

Under the parallel polarizers, the basal part appeared bright green in all directions of the incident polarization, as shown in Fig. 2(a). Correspondingly, the reflectance spectra showed a distinct peak at approximately 530 nm, as shown in Fig. 2(b). However, the width of the reflection band differed depending on the incident polarization. When the polarization angle was 0° (180°) from the x axis, the band was the broadest with the full width at half maximum (FWHM) of 67 nm, whereas at 90° , the peak became the narrowest with FWHM of 40 nm. The wavelength of this peak can be theoretically estimated from the Bragg condition $m\lambda = 2\bar{n}d$ under the normal incidence. Assuming the order m as 1, the wavelength λ was calculated as 550 nm from the following parameter values. The mean refractive index $\bar{n} \equiv n_{\text{cuticle}}\phi + n_{\text{air}}(1 - \phi)$ was calculated as the volume average as 1.23 with the refractive index of cuticle as $n_{\text{cuticle}} = 1.555$ and that of air as $n_{\text{air}} = 1.000$. The cuticle fraction ϕ was set to 0.423 based on the previously reported parameter value $t = 0.218$ in Eq. (1) (see the Method section) [41]. The plane distance d was set to $\frac{\sqrt{2}a}{2} = 223\ \text{nm}$ because the (110) plane was considered as $a = 315\ \text{nm}$ [41]. The calculated wavelength of 550 nm was in reasonable agreement with the peak wavelength of the reflectance spectra. The peak width difference depending on the polarization is discussed later.

When the scale was observed under the crossed polarizers, the reflection intensity showed large polarization dependence; for incident linear polarization at 0° and 90° , the scale appeared entirely dark and the reflectance was nearly zero (Fig. 3). In contrast, the scale appeared the brightest at 45° or 135° , and the reflectance spectra were observed to have two peaks at the wavelengths of approximately 510 and 560 nm. These peaks were roughly located at the two sides of the reflection peak observed under the parallel polarizers (Fig. S2; see the Supplemental Material) [45].

IV. ANALYSIS

The experiments on the polarization dependence showed two major characteristics for the case where light was incident on the (110) plane of the I-WP-type photonic crystal. First, the reflection bandwidth under the parallel polarizers differed depending on the polarization. Second, under the crossed polarizers, the reflectance spectrum had two peaks located on both sides of the reflection band observed under the parallel polarizers. In this section, these polarization properties are theoretically investigated based on the calculations of the photonic band diagram, assuming an infinitely large crystal and reflectance spectra from a finite-sized crystal, by using the RCWA method.

A. Photonic band calculation and mode symmetry

We calculated the photonic band diagram of the I-WP-type photonic crystal by using the plane-wave expansion method (Fig. 4) [43]. The I-WP-type photonic crystal has a body-centered cubic (BCC) lattice, and the light propagating along the $[110]$ direction corresponds to the modes between Γ and N in the photonic band diagram. At the point N, the photonic

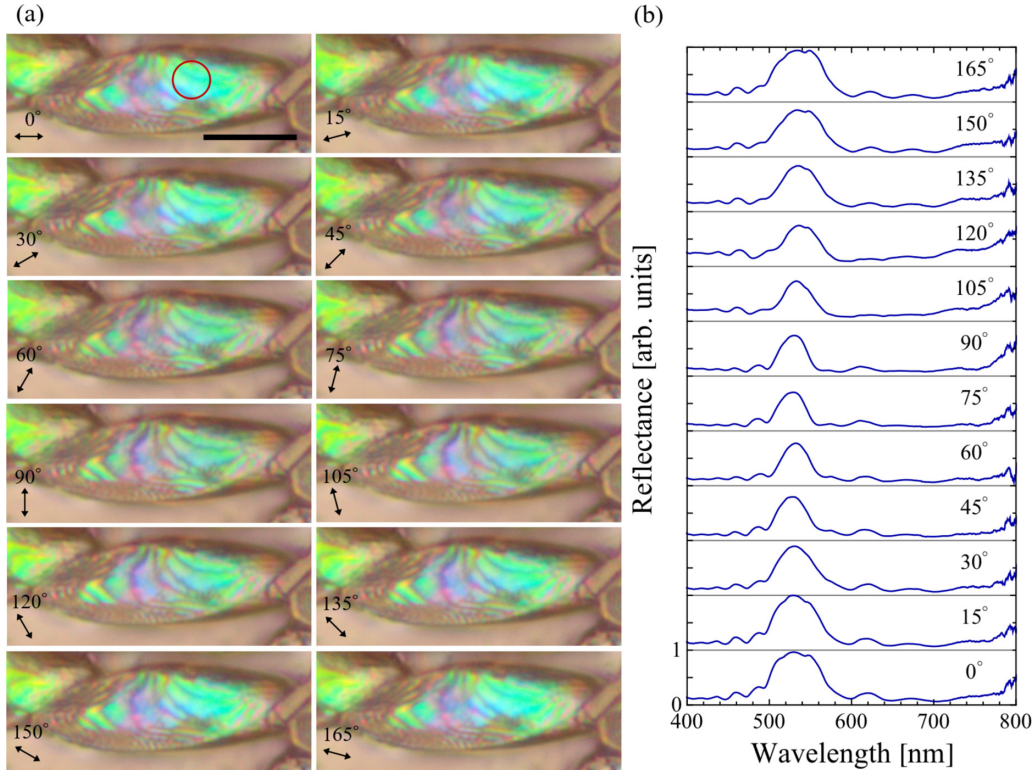


FIG. 2. Reflection properties under the parallel polarizers. (a) Optical micrographs of the scale when the angle of incident linear polarization is incremented successively by 15° . The direction and angle of the incident linear polarization are indicated in the lower left corner of the image. The scale bar is $10 \mu\text{m}$. (b) Reflectance spectra measured for the region indicated by the red circle in panel (a). To prevent the spectra from overlapping and becoming indistinguishable, the reflectance was vertically shifted by 1 for each angle of incident linear polarization.

band gap opens around the dimensionless frequency of $\frac{\omega a}{2\pi c} \approx 0.55$. However, it can be noticed that the electromagnetic (EM) modes at the upper and lower edges of the band gap split into two modes near N. We consider the lowest four EM modes between Γ and N from the first to fourth modes as the lowest to higher frequency modes. The symmetries of these four modes are associated with the local symmetry of the $[110]$ direction of the I-WP-type photonic crystal. This direction of the BCC lattice has a C_{2v} symmetry with four types of modes A_1 , A_2 , B_1 , and B_2 . According to the literature [50], the four EM modes propagating along the $[110]$ direction can be classified into the B_1 or B_2 mode. To determine the mode symmetry, we depicted the spatial patterns of the electric field vector (Fig. S3; see the Supplemental Material) [45] and found that the first and fourth modes are classified into the B_1 mode and the second and third modes as the B_2 mode, as indicated in the photonic band diagram. The B_1 mode is symmetric with respect to the mirror operation σ_{xz} and asymmetric with respect to the mirror operation σ_{yz} , whereas the reverse is true for the B_2 mode. When the y -polarized light is normally incident on the (110) plane, it can couple with only the B_2 mode, which has an electric field vector directed along the y axis. In contrast, the x -polarized light can couple with only the B_1 mode.

Figure 5 shows the comparison between the photonic band diagram and reflectance calculated for both the x - and y -polarized light. For the two polarization directions, the reflection band appears in the frequency ranges corresponding

to the band gaps for the B_1 and B_2 modes. It is noted that in the reflectance calculation, the thickness of the photonic crystal is assumed to be 20 periods along the $[110]$ direction; i.e., the thickness is $20 \times \sqrt{2}a$, which corresponds to 8910 nm with $a = 315$ nm. This thickness is used for the theoretical comparison with the photonic band diagram, assuming an infinitely large size, whereas the actual thickness of the scale is considered smaller than this.

B. Reflectance from a finite-sized photonic crystal

We theoretically investigated the polarization-dependent reflectance spectra under the parallel and crossed polarizers to compare the results with the experimental results shown in Figs. 2 and 3. By referring to a previous study [51], we calculated the reflectance spectra for the incident light polarizations from 0° to 180° at intervals of 15° . In the RCWA calculation, reflectance is obtained as the zeroth order diffraction coefficient. To express the polarization dependence, four reflection coefficients, r_{ij} ($i, j = x, y$), were considered, where the subscripts i and j represent the polarization direction of the incident and reflected light, respectively. From the four coefficients r_{xx} , r_{xy} , r_{yx} , and r_{yy} , we can calculate the parallel polarizers and crossed polarizers reflectances for any incident polarization angle as follows. When the angle between the polarization direction and x axis is θ , the electric field vector of the incidence is expressed as $\mathbf{E}_i = E_0(\cos \theta, \sin \theta, 0)$. The electric field vector of the reflected light becomes

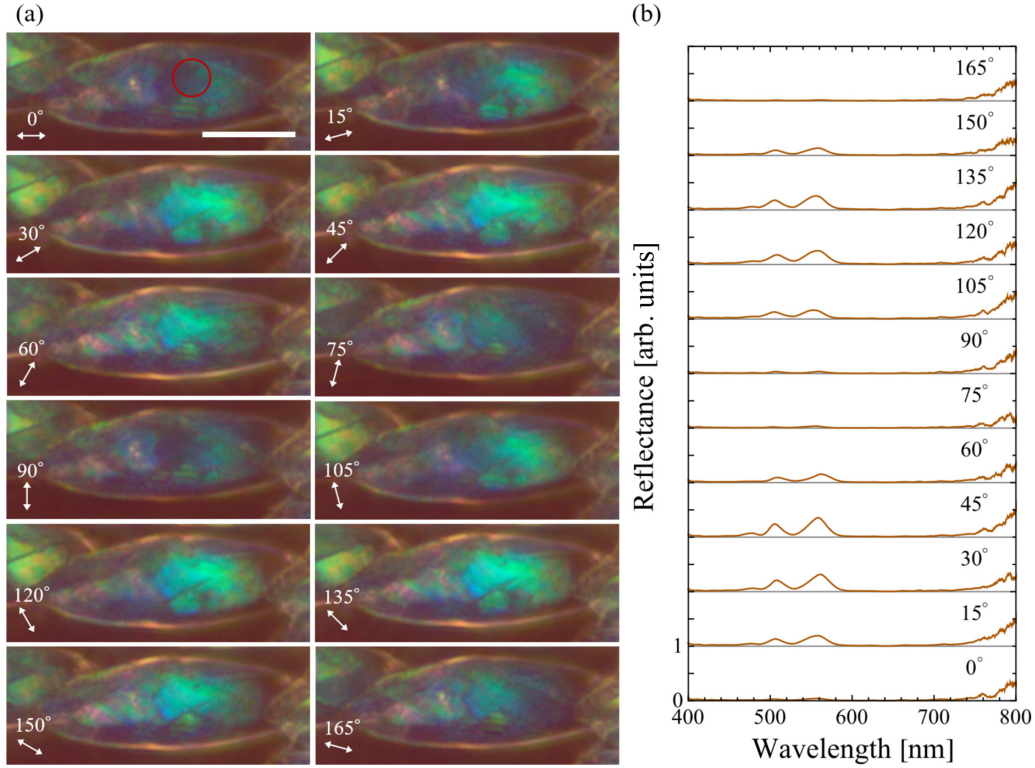


FIG. 3. Reflection properties under the crossed polarizers. (a) Optical micrographs of the scale when the angle of incident linear polarization is incremented successively by 15° . The direction and angle of the incident linear polarization are indicated in the lower left corner of the image. The scale bar is $10 \mu\text{m}$. (b) Reflectance spectra measured for the region indicated by the red circle in panel (a). To prevent the spectra from overlapping and becoming indistinguishable, the reflectance was vertically shifted by 1 for each angle of incident linear polarization.

$\mathbf{E}_r = E_0(r_{xx} \cos \theta + r_{yx} \sin \theta, r_{xy} \cos \theta + r_{yy} \sin \theta, 0)$. By using the two unit vectors $\mathbf{a}_{\parallel} = (\cos \theta, \sin \theta, 0)$ and $\mathbf{a}_{\perp} = (-\sin \theta, \cos \theta, 0)$, which are parallel and perpendicular to the incident light polarization, respectively, we can calculate the parallel and crossed polarizers reflectance coefficients as

$$r_{\parallel} \equiv \frac{\mathbf{E}_r \cdot \mathbf{a}_{\parallel}}{E_0} = r_{xx} \cos^2 \theta + r_{xy} \sin \theta \cos \theta + r_{yx} \sin \theta \cos \theta + r_{yy} \sin^2 \theta, \quad (2)$$

$$r_{\perp} \equiv \frac{\mathbf{E}_r \cdot \mathbf{a}_{\perp}}{E_0} = -r_{xx} \sin \theta \cos \theta + r_{xy} \cos^2 \theta - r_{yx} \sin^2 \theta + r_{yy} \sin \theta \cos \theta. \quad (3)$$

The reflectance is obtained as the absolute square of these reflection coefficients.

Figure 6 shows the reflectance spectra of the (a) parallel polarizers and (b) crossed polarizers when θ is successively incremented by 15° . The thickness of the crystal was assumed to be six periods along the [110] direction (2673 nm) so that the calculation moderately reproduced the positions of the side peaks in the experimental spectrum. In the case of the parallel polarizers, the reflection band was located at approximately 550 nm, but the width of the band changed depending on the polarization angle. In concurrence with the photonic band calculation, the width of the reflection band was the widest, approximately 520–580 nm, when the incident polarization was along the x axis, i.e., at $\theta = 0^\circ$ or 180° . The

reflection band became the narrowest, approximately 530–570 nm, when the polarization was along the y axis, i.e., at $\theta = 90^\circ$. In the crossed polarizers, the reflectance spectrum had two peaks at approximately 510 and 580 nm for the incident linear polarizations of 45° and 135° , respectively. These calculations reasonably reproduce the experimental results in Figs. 2 and 3. The difference in reflectance spectra under parallel and crossed polarizers can be briefly explained as the difference in the width of the band gap depending on the direction of incident polarization. The detailed interpretation is provided in the Discussion section.

V. DISCUSSION

In the Results and Analysis sections, we presented the experimental and theoretical results of the polarization-dependent reflective properties of a photonic crystal based on an I-WP-type minimal surface found in the scale of the longhorn beetle (*Sternotomis callais*). It was experimentally found that the width of the reflection band differed depending on the polarization direction. The theoretical calculation of the photonic band showed that the width of the band gap depends on the polarization, which is consistent with the experimental results. For the crossed polarizers, the spectral shape was found to have two peaks in both the experimental and theoretical results. Next, we discuss the physical origin of these optical properties and compare them with those observed in other natural systems.

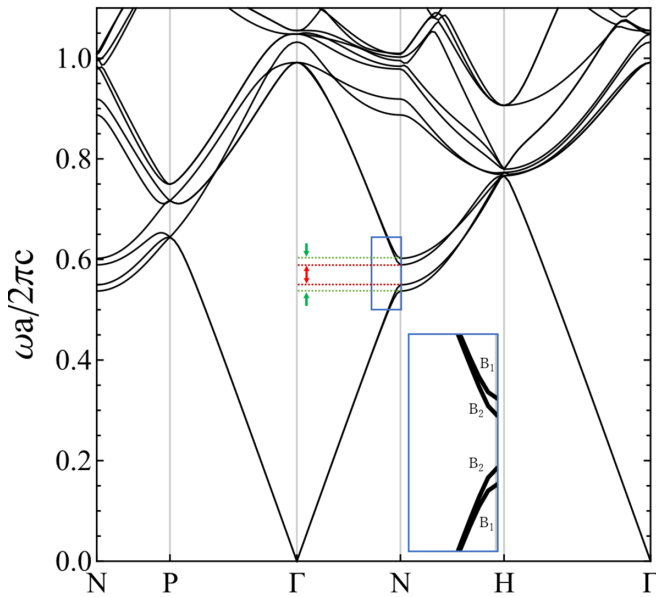


FIG. 4. Photonic band diagram of an I-WP-type photonic crystal. The band gap along the Γ -N direction opens near the frequency of $\frac{\omega a}{2\pi c} \approx 0.55$. The inset shows an enlarged view of the band gap area (blue rectangle). Symmetries of the modes are indicated (see text for details).

The (110) plane of the I-WP-type photonic crystal is characterized by the arrangement of oval-shaped holes, as shown in Fig. 1(f). Thus, the anisotropy of the oval shape and the resultant depolarization effect are important factors for the difference in the reflection bandwidth. That is, the depolarization field is stronger for the minor axis of the oval hole than the major axis, because the polarization charge is less separated along the direction of the minor axis, which is along the y axis. Bragg *et al.* examined the depolarization field and effective dielectric constant in prolate spheroids [52]. It was reported

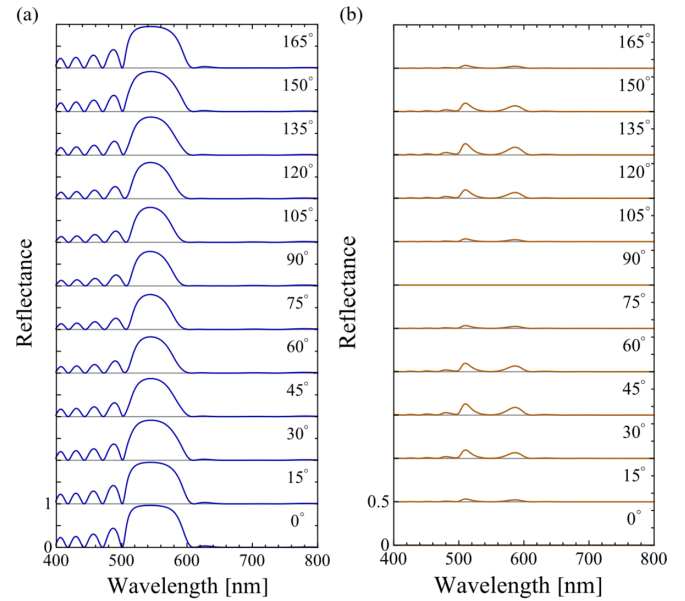


FIG. 6. Reflectance spectra of (a) parallel polarizers and (b) crossed polarizers for various directions of incident polarization. These spectra are calculated by the RCWA method. The reflectance is vertically shifted by (a) 1 and (b) 0.5 for each incident polarization angle to prevent overlapping.

that the depolarizing coefficient along the major axis of the prolate spheroids is smaller than that along the minor axis. This implies that the effective refractive index is larger along the major axis direction and smaller along the minor axis. In the case of a periodic multilayered structure consisting of two types of layers (one-dimensional photonic crystal), the band gap width generally depends on the refractive index contrast between the two materials. Similarly, in a three-dimensional photonic crystal, the degree of spatial variation in the effective refractive index along the propagation direction is

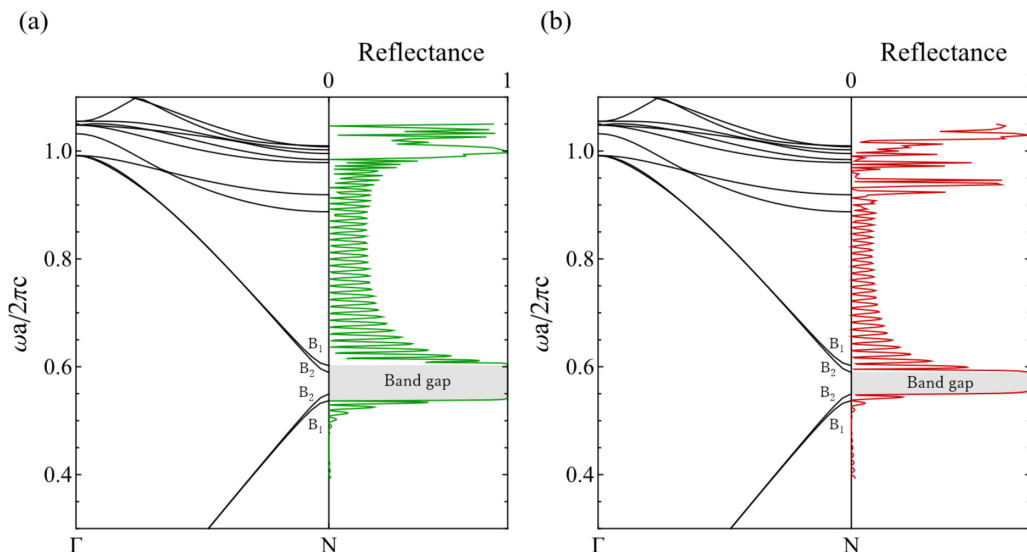


FIG. 5. Comparison of the Γ -N photonic band diagram (left panel) and reflectance spectra calculated by the RCWA method (right panel). The direction of the incident linear polarization is along the (a) x axis and (b) y axis.

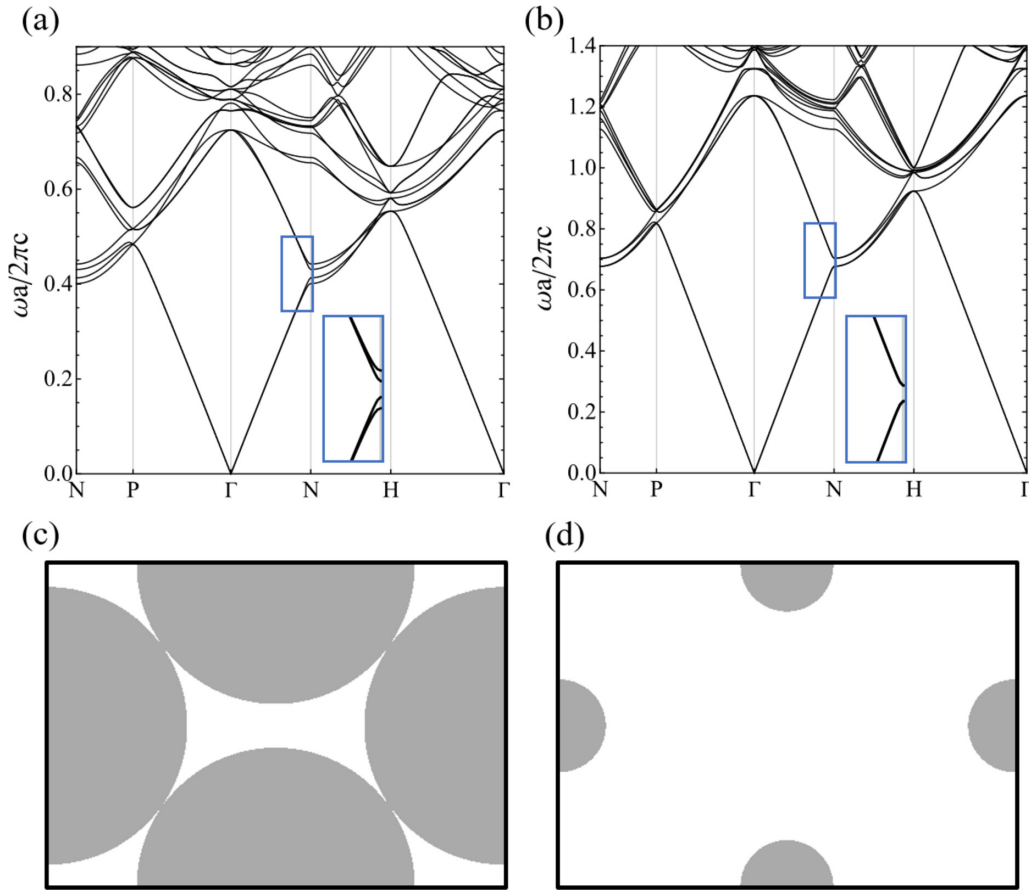


FIG. 7. Photonic band diagrams of (a) close-packed structure and (b) non-close-packed structure of the BCC lattice of spherical particles. The calculation was performed with the plane-wave expansion method using the reciprocal lattice points of 1055. The refractive indices were set to 2.00 and 1.00, and the filling fractions were (a) 0.680 and (b) 0.025, respectively. The inset shows an enlarged view of the band gap area (blue rectangle). Cross sections of the (110) plane in the (c) close-packed structure and (d) non-close-packed structure of the BCC lattice. Concave holes are found in the case of the close-packed structure, whereas they are not found in the case of the non-close-packed structure.

considered to affect the photonic band-gap width [39,53,54]. Thus, the anisotropy of the oval shape results in structural birefringence; accordingly, the different degrees of spatial variation are considered to affect the width of the photonic band gap, as supported by the reflection bands of different widths observed in the theoretical and experimental results.

Under the crossed polarizers, two separate peaks were observed, which were located on both sides of the reflection band under the parallel polarizers, as shown in Fig. S2 (see the Supplemental Material) [45]. It should be noted that such a spectrum is observed when the polarization is 45° from the x and y axes. In addition, a careful inspection reveals that the two peaks are located at the wavelengths corresponding to high reflectance for the x -polarized incidence and low reflectance for the y -polarized light under the parallel polarizers. Thus, we can interpret the origin of the two peaks under the crossed polarizers as follows: The electric field of the incident light of the polarization angle at 45° is decomposed into x and y components, and both components exist in the band gap for the B_2 mode, which is narrower than that of the B_1 mode. However, only the x component is strongly reflected for the frequency range contained in the band gap of the B_1 mode but not in the B_2 mode. In this frequency range, the

reflected light is x -polarized light, which is again decomposed into parallel and perpendicular components with respect to the incident polarization, and the perpendicular component is observed under the crossed polarizers.

Different polarization effects have been reported in other insects. For example, a tilted multilayer structure causes the rotation of the polarization [34–36] due to the oblique incidence and dual reflection from the multilayers. In weevil species, the scale has a diamond-type photonic crystal, which has a face-centered cubic (FCC) lattice. The (111) planes cause reflection at the longest wavelength in this structure. However, the (200) planes also cause Bragg reflection with the polarization conversion effect [37]. This effect is explained using the analogy of a half-wave phase shift [38]. The polarization properties reported in this paper are similar to those of the gyroid photonic crystals in the butterfly wing scale, because both the gyroid and I-WP photonic crystal have the BCC lattice and the Bragg diffraction from the (110) planes occurs at the longest wavelength. It has been reported that a gyroid-type structure has a reflectance spectrum with two peaks under the crossed polarizers [51]. However, the reflectance value is smaller than that in the case of the I-WP structure. In the gyroid structure, the two high-frequency modes and two low-frequency modes that correspond to the upper and lower

edges of the band gap, respectively, are not separate but almost degenerate (Fig. S4, see the Supplemental Material) [45], unlike those in the I-WP-type photonic crystal. The cross section of the (110) plane of the gyroid-type photonic crystal has air holes. However, these are nearly circular, not oval. The difference in the degree of structural anisotropy is considered to result in different reflectance values.

From the biological viewpoint, it is presumed that minimal-surface-based photonic crystals are created through the folding of the biological membrane and subsequent secretion of nascent cuticle, which later becomes dry cuticle [21]. It may not be easy to directly apply this concept to artificial production of the photonic crystal. Hence, we consider a different photonic structure that can be produced through a different process but has a similar polarization effect. The I-WP-type photonic crystal contains an interconnecting network of BCC lattice sites [Fig. 1(e)]. This structure is similar to that of the close-packed BCC lattice consisting of spherical particles. Although spherical colloidal particles generally form the FCC lattice, the BCC lattice has been reported in systems with low volume fraction and long Debye screening lengths [55,56]. We calculated the photonic band diagram for the close-packed BCC lattice consisting of spherical particles with refractive index same as that of the cuticle. The results showed that the EM modes between Γ and N were separated near N and had very similar optical characteristics to those of the I-WP-type photonic crystals (Fig. 7). In fact, the (110) plane of the BCC close-packed structure appears as an arrangement of concave holes, which are elongated along one direction. These elongated holes are considered to cause structural birefringence, which separates the EM modes as in the I-WP photonic crystal structure. It was confirmed that for a non-close-packed structure, the EM modes are not separated (Fig. 7). It may be possible to enhance the reflectance and increase the photonic bandwidth by using different materials with higher

refractive index values for the artificial colloidal photonic crystal.

VI. CONCLUSION

In this study, we experimentally and theoretically investigated the polarization-dependent reflection of the I-WP-type photonic crystal discovered recently in the scales of the longhorn beetle (*Sternotomis callais*). It was found that the width of the reflection band under the parallel polarizers differed depending on the polarization, whereas a spectral shape with two reflection peaks was observed under the crossed polarizers. These features were theoretically reproduced and explained based on the structural birefringence originating from the oval shaped holes in the (110) plane of the I-WP photonic crystal.

Similar to the recent discovery of the I-WP structure, differently shaped photonic crystals may be discovered in the future. It is important to investigate their optical properties to inspire the development of new optical materials. From the biological viewpoint, butterflies and mantis shrimps are known to have polarization-sensitive vision. Hence, the polarized light is considered to play a role in courtship signals and foraging [57,58]. Understanding the polarization properties of the natural structural color may provide clues to explain why animals develop specific nanostructures.

ACKNOWLEDGMENTS

This work was supported by Grant-in-Aid for Scientific Research No. 18H01191 from the Ministry of Education, Culture, Sports, Science, and Technology (MEXT, Japan). R.O. performed the theoretical analysis. Y.K. conducted the experiments. R.O. and S.Y. wrote the manuscript.

-
- [1] M. Srinivasarao, Nano-optics in the biological world: Beetles, butterflies, birds, and moths, *Chem. Rev.* **99**, 1935 (1999).
 - [2] P. Vukusic and J. R. Sambles, Photonic structures in biology, *Nature (London)* **424**, 852 (2003).
 - [3] S. Kinoshita and S. Yoshioka, Structural colors in nature: The role of regularity and irregularity in the structure, *Chem. Phys. Chem.* **6**, 1442 (2005).
 - [4] S. Kinoshita, S. Yoshioka, and J. Miyazaki, Physics of structural colors, *Rep. Prog. Phys.* **71**, 076401 (2008).
 - [5] J. A. Noyes, P. Vukusic, and I. R. Hooper, Experimental method for reliably establishing the refractive index of buprestid beetle exocuticle, *Opt. Express* **15**, 4351 (2007).
 - [6] D. G. Stavenga, B. D. Wilts, H. L. Leertouwer, and T. Hariyama, Polarized iridescence of the multilayered elytra of the Japanese jewel beetle, *Chrysochroa fulgidissima*, *Phil. Trans. R. Soc. B* **366**, 709 (2011).
 - [7] S. Yoshioka, S. Kinoshita, H. Iida, and T. Hariyama, Phase-adjusting layers in the multilayer reflector of a jewel beetle, *J. Phys. Soc. Jpn.* **81**, 054801 (2012).
 - [8] S. Kinoshita, S. Yoshioka, and K. Kawagoe, Mechanisms of structural colour in the morpho butterfly: Cooperation of regularity and irregularity in an iridescent scale, *Proc. R. Soc. London B* **269**, 1417 (2002).
 - [9] S. Yoshioka and S. Kinoshita, Single-scale spectroscopy of structurally colored butterflies: Measurements of quantified reflectance and transmittance, *J. Opt. Soc. Am. A* **23**, 134 (2006).
 - [10] M. A. Giraldo and D. G. Stavenga, Brilliant iridescence of *Morpho* butterfly wing scales is due to both a thin film lower lamina and a multilayered upper lamina, *J. Comp. Physiol. A* **202**, 381 (2016).
 - [11] S. Yoshioka, E. Nakamura, and S. Kinoshita, Origin of two-color iridescence in rock dove's feather, *J. Phys. Soc. Jpn.* **76**, 013801 (2007).
 - [12] H. Yin, L. Shi, J. Sha, Y. Li, Y. Qin, B. Dong, S. Meyer, X. Liu, L. Zhao, and J. Zi, Iridescence in the neck feathers of domestic pigeons, *Phys. Rev. E* **74**, 051916 (2006).
 - [13] J. A. Dolan, B. D. Wilts, S. Vignolini, J. J. Baumberg, U. Steiner, and T. D. Wilkinson, Optical properties of gyroid structured materials: From photonic crystals to metamaterials, *Adv. Opt. Mater.* **3**, 12 (2015).
 - [14] L. Han and S. Che, An overview of materials with triply periodic minimal surfaces and related geometry: From biological

- structures to self-assembled systems, *Adv. Mater.* **30**, 1705708 (2018).
- [15] J. W. Galusha, L. R. Richey, J. S. Gardner, J. N. Cha, and M. H. Bartl, Discovery of a diamond-based photonic crystal structure in beetle scales, *Phys. Rev. E* **77**, 050904(R) (2008).
- [16] B. D. Wilts, K. Michielsen, H. De Raedt, and D. G. Stavenga, Hemispherical Brillouin zone imaging of a diamond-type biological photonic crystal, *J. R. Soc. Interface* **9**, 1609 (2012).
- [17] V. Saranathan, A. E. Seago, A. Sandy, S. Narayanan, S. G. Mochrie, E. R. Dufresne, H. Cao, C. O. Osuji, and R. O. Prum, Structural diversity of arthropod biophotonic nanostructures spans amphiphilic phase-space, *Nano Lett.* **15**, 3735 (2015).
- [18] R. Ebihara, H. Hashimoto, J. Kano, T. Fujii, and S. Yoshioka, Cuticle network and orientation preference of photonic crystals in the scales of the weevil *Lamprocyphus augustus*, *J. R. Soc. Interface* **15**, 20180360 (2018).
- [19] B. D. Wilts and V. Saranathan, A literal elytral rainbow: Tunable structural colors using single diamond biophotonic crystals in *Pachyrrhynchus congestus* weevils, *Small* **14**, 1802328 (2018).
- [20] K. Michielsen and D. G. Stavenga, Gyroid cuticular structures in butterfly wing scales: Biological photonic crystals, *J. R. Soc. Interface* **5**, 85 (2008).
- [21] V. Saranathan, C. O. Osuji, S. G. Mochrie, H. Noh, S. Narayanan, A. Sandy, E. R. Dufresne, and R. O. Prum, Structure, function, and self-assembly of single network gyroid (14,32) photonic crystals in butterfly wing scales, *Proc. Natl. Acad. Sci. USA* **107**, 11676 (2010).
- [22] G. E. Schröder-Turk, S. Wickham, H. Averdunk, F. Brink, J. D. F. Gerald, L. Poladian, M. C. J. Large, and S. T. Hyde, The chiral structure of porous chitin within the wing-scales of *Callophrys rubi*, *J. Struct. Biol.* **174**, 290 (2011).
- [23] A. Singer, L. Boucheron, S. H. Dietze, K. E. Jensen, D. Vine, I. McNulty, E. R. Dufresne, R. O. Prum, S. G. Mochrie, and O. G. Shpyrko, Domain morphology, boundaries, and topological defects in biophotonic gyroid nanostructures of butterfly wing scales, *Sci. Adv.* **2**, e1600149 (2016).
- [24] R. W. Corkery and E. C. Tyrode, On the colour of wing scales in butterflies: Iridescence and preferred orientation of single gyroid photonic crystals, *Interface Focus* **7**, 20160154 (2017).
- [25] M. Maldovan, A. M. Urbas, N. Yufa, W. C. Carter, and E. L. Thomas, Photonic properties of bicontinuous cubic microphases, *Phys. Rev. B* **65**, 165123 (2002).
- [26] M. Saba, M. Thiel, M. D. Turner, S. T. Hyde, M. Gu, K. Grosse-Brauckmann, D. N. Neshev, K. Mecke, and G. E. Schröder-Turk, Circular Dichroism in Biological Photonic Crystals and Cubic Chiral Nets, *Phys. Rev. Lett.* **106**, 103902 (2011).
- [27] S. S. Oh, A. Demetriadou, S. Wuestner, and O. Hess, On the origin of chirality in nanoplasmonic gyroid metamaterials, *Adv. Mater.* **25**, 612 (2013).
- [28] C. Mille, E. C. Tyrode, and R. W. Corkery, Inorganic chiral 3-D photonic crystals with bicontinuous gyroid structure replicated from butterfly wing scales, *Chem. Commun.* **47**, 9873 (2011).
- [29] C. Mille, E. C. Tyrode, and R. W. Corkery, 3D titania photonic crystals replicated from gyroid structures in butterfly wing scales: Approaching full band gaps at visible wavelengths, *RSC Adv.* **3**, 3109 (2013).
- [30] B. P. Cumming, M. D. Turner, G. E. Schröder-Turk, S. Debbarma, B. Luther-Davies, and M. Gu, Adaptive optics enhanced direct laser writing of high refractive index gyroid photonic crystals in chalcogenide glass, *Opt. Express* **22**, 689 (2014).
- [31] M. D. Turner, G. E. Schröder-Turk, and M. Gu, Fabrication and characterization of three-dimensional biomimetic chiral composites, *Opt. Express* **19**, 10001 (2011).
- [32] M. D. Turner, M. Saba, Q. Zhang, B. P. Cumming, G. E. Schröder-Turk, and M. Gu, Miniature chiral beamsplitter based on gyroid photonic crystals, *Nat. Photon.* **7**, 801 (2013).
- [33] B. D. Wilts, B. Apeleo Zubiri, M. A. Klatt, B. Butz, M. G. Fischer, S. T. Kelly, E. Spiecker, U. Steiner, and G. E. Schröder-Turk, Butterfly gyroid nanostructures as a time-frozen glimpse of intracellular membrane development, *Sci. Adv.* **3**, e1603119 (2017).
- [34] P. Vukusic, J. R. Sambles, and C. Lawrence, Colour mixing in wing scales of a butterfly, *Nature (London)* **404**, 457 (2000).
- [35] P. Vukusic, R. Sambles, C. Lawrence, and G. Wakely, Sculpted-multilayer optical effects in two species of *Papilio* butterfly, *Appl. Opt.* **40**, 1116 (2001).
- [36] S. Yoshioka and S. Kinoshita, Polarization-sensitive color mixing in the wing of the Madagascan sunset moth, *Opt. Express* **15**, 2691 (2007).
- [37] X. Wu, F. L. Rodríguez-Gallegos, M.-C. Heep, B. Schwind, G. Li, H.-O. Fabritius, G. von Freymann, and J. Förstner, Polarization conversion effect in biological and synthetic photonic diamond structures, *Adv. Opt. Mater.* **6**, 1800635 (2018).
- [38] S. Imagawa and K. Edagawa, Polarization conversion by a three-dimensional photonic crystal mirror with a diamond structure, *Photon. Nanostructures* **10**, 281 (2012).
- [39] S. Yoshioka, H. Fujita, S. Kinoshita, and B. Matsuhana, Alignment of crystal orientations of the multi-domain photonic crystals in *Parides sesostris* wing scales, *J. R. Soc. Interface* **11**, 20131029 (2014).
- [40] B. D. Wilts, K. Michielsen, H. De Raedt, and D. G. Stavenga, Iridescence and spectral filtering of the gyroid-type photonic crystals in *Parides sesostris* wing scales, *Interface Focus* **2**, 681 (2012).
- [41] Y. Kobayashi, R. Ohnuki, and S. Yoshioka, Discovery of I-WP minimal-surface-based photonic crystal in the scale of a longhorn beetle, *J. R. Soc. Interface* **18**, 20210505 (2021).
- [42] D. M. Anderson, H. T. Davis, E. L. Scriven, and J. C. C. Nitsche, *Periodic Surfaces of Prescribed Mean Curvature*, Advances in Chemical Physics Vol. 77 (John Wiley & Sons, Hoboken, 1990).
- [43] K. M. Ho, C. T. Chan, and C. M. Soukoulis, Existence of a Photonic Gap in Periodic Dielectric Structures, *Phys. Rev. Lett.* **65**, 3152 (1990).
- [44] The Becke line test indicated that the refractive index of the cuticle is between 1.55 and 1.56. Their average, 1.555, was used for the calculation.
- [45] See the Supplemental Material at <http://link.aps.org/supplemental/10.1103/PhysRevE.106.014123> for mathematical derivation of I-WP minimal-surface-based photonic crystal and figures that support the main text, which includes Refs. [46] and [47].
- [46] U. S. Schwarz and G. Gompper, Systematic approach to bicontinuous cubic phases in ternary amphiphilic systems, *Phys. Rev. E* **59**, 5528 (1999).

- [47] H. G. Von Schnering and R. Nesper, Nodal surfaces of Fourier series: Fundamental invariants of structured matter, *Z. Phys. B* **83**, 407 (1991).
- [48] M. G. Moharam, E. B. Grann, D. A. Pommet, and T. K. Gaylord, Formulation for stable and efficient implementation of the rigorous coupled-wave analysis of binary gratings, *J. Opt. Soc. Am. A* **12**, 1068 (1995).
- [49] M. G. Moharam, D. A. Pommet, E. B. Grann, and T. K. Gaylord, Stable implementation of the rigorous coupled-wave analysis for surface-relief gratings: Enhanced transmittance matrix approach, *J. Opt. Soc. Am. A* **12**, 1077 (1995).
- [50] K. Sakoda, *Optical Properties of Photonic Crystals*, Optical Sciences Vol. 80 (Springer Science & Business Media, Berlin, 2004).
- [51] S. Yoshioka, B. Matsuhana, and H. Fujita, Polarization-dependent tessellated pattern of the wing scale of the *Parides sesostris* butterfly, *Mater. Today: Proc.* **1**, 186 (2014).
- [52] W. L. Bragg and A. B. Pippard, The form birefringence of macromolecules, *Acta Crystallogr.* **6**, 865 (1953).
- [53] N. Vogel, S. Utech, G. T. England, T. Shirman, K. R. Phillips, N. Koay, I. B. Burgess, M. Kolle, D. A. Weitz, and J. Aizenberg, Color from hierarchy: Diverse optical properties of micron-sized spherical colloidal assemblies, *Proc. Natl. Acad. Sci. USA* **112**, 10845 (2015).
- [54] R. Ohnuki, M. Sakai, Y. Takeoka, and S. Yoshioka, Detailed analysis of peripheral reflection from a photonic ball, *Adv. Photon. Res.* **2**, 2100131 (2021).
- [55] S. Arai and H. Tanaka, Surface-assisted single-crystal formation of charged colloids, *Nat. Phys.* **13**, 503 (2017).
- [56] Y. Chen, Z. Yao, S. Tang, H. Tong, T. Yanagishima, H. Tanaka, and P. Tan, Morphology selection kinetics of crystallization in a sphere, *Nat. Phys.* **17**, 121 (2021).
- [57] I. M. Daly, M. J. How, J. C. Partridge, S. E. Temple, N. J. Marshall, T. W. Cronin, and N. W. Roberts, Dynamic polarization vision in mantis shrimps, *Nat. Commun.* **7**, 12140 (2016).
- [58] K. Zhang, Y. Tang, J. Meng, G. Wang, H. Zhou, T. Fan, and D. Zhang, Polarization-sensitive color in butterfly scales: Polarization conversion from ridges with reflecting elements, *Opt. Express* **22**, 27437 (2014).